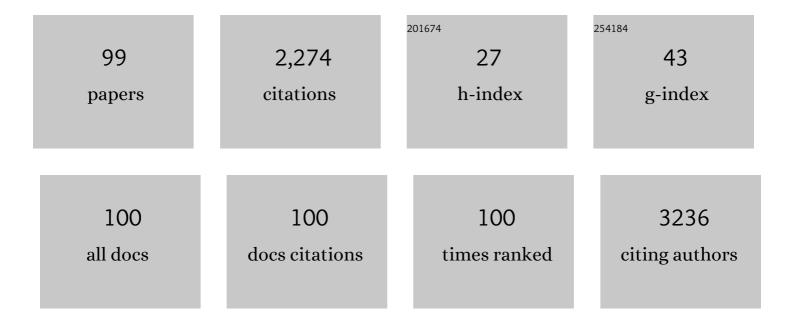
List of Publications by Year in descending order

Source: https://exaly.com/author-pdf/8911604/publications.pdf Version: 2024-02-01



#	Article	IF	CITATIONS
1	3D-micro-MR angiography of mice using macromolecular MR contrast agents with polyamidoamine dendrimer core with reference to their pharmacokinetic properties. Magnetic Resonance in Medicine, 2001, 45, 454-460.	3.0	143
2	Pharmacokinetics and enhancement patterns of macromolecular MR contrast agents with various sizes of polyamidoamine dendrimer cores. Magnetic Resonance in Medicine, 2001, 46, 1169-1173.	3.0	127
3	Ovarian cancer: the clinical role of US, CT, and MRI. European Radiology, 2003, 13, L87-L104.	4.5	111
4	Intravoxel Incoherent Motion and Quantitative Non-Gaussian Diffusion MR Imaging: Evaluation of the Diagnostic and Prognostic Value of Several Markers of Malignant and Benign Breast Lesions. Radiology, 2018, 287, 432-441.	7.3	93
5	Microâ€MR angiography of normal and intratumoral vessels in mice using dedicated intravascular MR contrast agents with high generation of polyamidoamine dendrimer core: Reference to pharmacokinetic properties of dendrimerâ€based MR contrast agents. Journal of Magnetic Resonance Imaging, 2001, 14, 705-713.	3.4	86
6	Regulation of <sup>18</sup> F-FDG Accumulation in Colorectal Cancer Cells with Mutated <i>KRAS</i> . Journal of Nuclear Medicine, 2014, 55, 2038-2044.	5.0	65
7	Uterine contractions: Possible diagnostic pitfall at MR imaging. Journal of Magnetic Resonance Imaging, 1993, 3, 889-893.	3.4	62
8	Visualising peripheral arterioles and venules through high-resolution and large-area photoacoustic imaging. Scientific Reports, 2018, 8, 14930.	3.3	62
9	Usefulness of gradient tree boosting for predicting histological subtype and EGFR mutation status of non-small cell lung cancer on 18F FDG-PET/CT. Annals of Nuclear Medicine, 2020, 34, 49-57.	2.2	62
10	Quantitative Susceptibility Mapping at 3 T and 1.5 T. Investigative Radiology, 2015, 50, 522-530.	6.2	58
11	Anatomy and physiology of the female pelvis: MR imaging revisited. Journal of Magnetic Resonance Imaging, 2001, 13, 842-849.	3.4	55
12	Environmental Risk Factors for Pulmonary Mycobacterium avium-intracellulare Complex Disease. Chest, 2011, 140, 723-729.	0.8	54
13	Clinical Report on the First Prototype of a Photoacoustic Tomography System with Dual Illumination for Breast Cancer Imaging. PLoS ONE, 2015, 10, e0139113.	2.5	53
14	Invited. Cervical cancer. Journal of Magnetic Resonance Imaging, 1998, 8, 391-397.	3.4	52
15	Real-time 3D Photoacoustic Visualization System with a Wide Field of View for Imaging Human Limbs. F1000Research, 2018, 7, 1813.	1.6	52
16	Relationship Between <sup>18</sup> F-FDG PET/CT Scans and <i>KRAS</i> Mutations in Metastatic Colorectal Cancer. Journal of Nuclear Medicine, 2015, 56, 1322-1327.	5.0	48
17	3D MR angiography of intratumoral vasculature using a novel macromolecular MR contrast agent. Magnetic Resonance in Medicine, 2001, 46, 579-585.	3.0	45
18	Novel intravascular macromolecular MRI contrast agent with generation-4 polyamidoamine dendrimer core: Accelerated renal excretion with coinjection of lysine. Magnetic Resonance in Medicine, 2001, 46, 457-464.	3.0	41

#	Article	IF	CITATIONS
19	Magnetic resonance angiography with compressed sensing: An evaluation of moyamoya disease. PLoS ONE, 2018, 13, e0189493.	2.5	36
20	MR imaging of the ovaries: normal appearance and benign disease. Radiologic Clinics of North America, 2003, 41, 799-811.	1.8	33
21	Uterine Contractility Evaluated on Cine Magnetic Resonance Imaging. Annals of the New York Academy of Sciences, 2007, 1101, 62-71.	3.8	33
22	<sup>18</sup> F-Labeled Phenyldiazenyl Benzothiazole for in Vivo Imaging of Neurofibrillary Tangles in Alzheimer's Disease Brains. ACS Medicinal Chemistry Letters, 2012, 3, 58-62.	2.8	33
23	Prevalence and risk factors for chronic co-infection in pulmonary <i>Mycobacterium avium</i> complex disease. BMJ Open Respiratory Research, 2014, 1, e000050.	3.0	32
24	FRET-assisted photoactivation of flavoproteins for in vivo two-photon optogenetics. Nature Methods, 2019, 16, 1029-1036.	19.0	32
25	MR imaging findings of ovarian torsion correlate with pathological hemorrhagic infarction. Journal of Obstetrics and Gynaecology Research, 2015, 41, 1433-1439.	1.3	31
26	Quantitative measurement of airway dimensions using ultra-high resolution computed tomography. Respiratory Investigation, 2018, 56, 489-496.	1.8	31
27	Primary central nervous system lymphoma and glioblastoma: differentiation using dynamic susceptibility-contrast perfusion-weighted imaging, diffusion-weighted imaging, and 18F-fluorodeoxyglucose positron emission tomography. Clinical Imaging, 2015, 39, 390-395.	1.5	30
28	Timeâ€dependent diffusion MRI to distinguish malignant from benign head and neck tumors. Journal of Magnetic Resonance Imaging, 2019, 50, 88-95.	3.4	30
29	Subendometrial enhancement and peritumoral enhancement for assessing endometrial cancer on dynamic contrast enhanced MR imaging. European Journal of Radiology, 2015, 84, 581-589.	2.6	28
30	Temporal Subtraction of Serial CT Images with Large Deformation Diffeomorphic Metric Mapping in the Identification of Bone Metastases. Radiology, 2017, 285, 629-639.	7.3	28
31	Vascular branching point counts using photoacoustic imaging in the superficial layer of the breast: A potential biomarker for breast cancer. Photoacoustics, 2018, 11, 6-13.	7.8	28
32	Structure–Activity Relationships and in Vivo Evaluation of Quinoxaline Derivatives for PET Imaging of β-Amyloid Plaques. ACS Medicinal Chemistry Letters, 2013, 4, 596-600.	2.8	25
33	Prediction of clinical outcome after stereotactic body radiotherapy for non-small cell lung cancer using diffusion-weighted MRI and 18F-FDC PET. European Journal of Radiology, 2014, 83, 2087-2092.	2.6	25
34	Feasibility and diagnostic performance of fractional flow reserve measurement derived from coronary computed tomography angiography in real clinical practice. International Journal of Cardiovascular Imaging, 2017, 33, 271-281.	1.5	25
35	Brain MRI with Quantitative Susceptibility Mapping: Relationship to CT Attenuation Values. Radiology, 2020, 294, 600-609.	7.3	20
36	Uterine Peristalsis in Women With Repeated IVF Failures: Possible Therapeutic Effect of Hyoscine Bromide. Journal of Obstetrics and Gynaecology Canada, 2009, 31, 732-735.	0.7	19

#	Article	IF	CITATIONS
37	Evaluation of Malignant Breast Lesions Using High-resolution Readout-segmented Diffusion-weighted Echo-planar Imaging: Comparison with Pathology. Magnetic Resonance in Medical Sciences, 2021, 20, 204-215.	2.0	17
38	Optimization of Regularization Parameters in Compressed Sensing of Magnetic Resonance Angiography: Can Statistical Image Metrics Mimic Radiologists' Perception?. PLoS ONE, 2016, 11, e0146548.	2.5	17
39	Comparative evaluation of respiratory-gated and ungated FDG-PET for target volume definition in radiotherapy treatment planning for pancreatic cancer. Radiotherapy and Oncology, 2016, 120, 217-221.	0.6	16
40	Quantitative and Qualitative Evaluation of Convolutional Neural Networks with a Deeper U-Net for Sparse-View Computed Tomography Reconstruction. Academic Radiology, 2020, 27, 563-574.	2.5	16
41	Prognostic Value of Quantitative Parameters of <sup>18</sup> F-FDG PET/CT for Patients With Angiosarcoma. American Journal of Roentgenology, 2020, 214, 649-657.	2.2	16
42	Polysplenia associated with semiannular pancreas. European Radiology, 2001, 11, 1639-1641.	4.5	15
43	Obstructive sleep apnea and abdominal aortic calcification: Is there anÂassociation independent of comorbid risk factors?. Atherosclerosis, 2015, 241, 6-11.	0.8	15
44	Complementary regional heterogeneity information from COPD patients obtained using oxygen-enhanced MRI and chest CT. PLoS ONE, 2018, 13, e0203273.	2.5	14
45	Distinguishing intrahepatic mass-forming biliary carcinomas from hepatocellular carcinoma by computed tomography and magnetic resonance imaging using the Bayesian method: a bi-center study. European Radiology, 2020, 30, 5992-6002.	4.5	14
46	MRI findings of isolated tubal torsions: case series of 12 patients. Clinical Imaging, 2017, 41, 28-32.	1.5	13
47	Addition of Amide Proton Transfer Imaging to FDG-PET/CT Improves Diagnostic Accuracy in Glioma Grading: A Preliminary Study Using the Continuous Net Reclassification Analysis. American Journal of Neuroradiology, 2018, 39, 265-272.	2.4	13
48	The comparison of high-resolution diffusion weighted imaging (DWI) with high-resolution contrast-enhanced MRI in the evaluation of breast cancers. Magnetic Resonance Imaging, 2020, 71, 161-169.	1.8	13
49	Assessment of treatment response after lung stereotactic body radiotherapy using diffusion weighted magnetic resonance imaging and positron emission tomography: A pilot study. European Journal of Radiology, 2017, 92, 58-63.	2.6	12
50	Predictability of <sup>99m</sup> Tc-Galactosyl Human Serum Albumin Scintigraphy for Posthepatectomy Liver Failure. American Journal of Roentgenology, 2018, 210, 158-165.	2.2	12
51	First-in-Human Evaluation of Positron Emission Tomography/Computed Tomography With [18F]FB(ePEG12)12-Exendin-4: A Phase 1 Clinical Study Targeting GLP-1 Receptor Expression Cells in Pancreas. Frontiers in Endocrinology, 2021, 12, 717101.	3.5	12
52	A study of computer-aided diagnosis for pulmonary nodule: comparison between classification accuracies using calculated image features and imaging findings annotated by radiologists. International Journal of Computer Assisted Radiology and Surgery, 2017, 12, 767-776.	2.8	11
53	Evaluation of image quality of pituitary dynamic contrastâ€enhanced MRI using timeâ€resolved angiography with interleaved stochastic trajectories (TWIST) and iterative reconstruction TWIST (ITâ€TWIST). Journal of Magnetic Resonance Imaging, 2020, 51, 1497-1506.	3.4	11
54	Inflammation-induced synergetic enhancement of nanoparticle treatments with DOXIL® and 90Y-Lactosome for orthotopic mammary tumor. Journal of Nanoparticle Research, 2016, 18, 1.	1.9	10

#	Article	IF	CITATIONS
55	Evaluation of Tumor-associated Stroma and Its Relationship with Tumor Hypoxia Using Dynamic Contrast-enhanced CT and18F Misonidazole PET in Murine Tumor Models. Radiology, 2016, 278, 734-741.	7.3	10
56	Synthesis and biological evaluation of F-18 labeled tetrahydroisoquinoline derivatives targeting orexin 1 receptor. Bioorganic and Medicinal Chemistry Letters, 2019, 29, 1620-1623.	2.2	10
57	Initial evaluation of PET / CT with 18 F―FSU â€880 targeting prostateâ€specific membrane antigen in prostate cancer patients. Cancer Science, 2019, 110, 742-750.	3.9	10
58	Prognostic utility of FDG PET/CT in advanced ovarian, fallopian and primary peritoneal high-grade serous cancer patients before and after neoadjuvant chemotherapy. Annals of Nuclear Medicine, 2020, 34, 128-135.	2.2	10
59	Additional benefit of computed diffusion-weighted imaging for detection of hepatic metastases at 1.5T. Clinical Imaging, 2016, 40, 481-485.	1.5	9
60	Internal evaluation of impregnation treatment of waterlogged wood; relation between concentration of internal materials and relaxation time using magnetic resonance imaging. Magnetic Resonance Imaging, 2017, 38, 196-201.	1.8	9
61	Effect of long fasting on myocardial accumulation in 18F-fluorodeoxyglucose positron emission tomography after chemoradiotherapy for esophageal carcinoma. Journal of Radiation Research, 2018, 59, 182-189.	1.6	9
62	18F-labeled benzimidazopyridine derivatives for PET imaging of tau pathology in Alzheimer's disease. Bioorganic and Medicinal Chemistry, 2019, 27, 3587-3594.	3.0	9
63	CT and MR imaging findings of systemic complications occurring during pregnancy and puerperal period, adversely affected by natural changes. European Journal of Radiology Open, 2015, 2, 101-110.	1.6	8
64	Evaluation of uterine peristalsis using cine MRI on the coronal plane in comparison with the sagittal plane. Acta Radiologica, 2016, 57, 122-127.	1.1	8
65	Conversion of iodine to fluorine-18 based on iodinated chalcone and evaluation for β-amyloid PET imaging. Bioorganic and Medicinal Chemistry, 2018, 26, 3352-3358.	3.0	8
66	Increased 14C-acetate accumulation in IDH-mutated human glioblastoma: implications for detecting IDH-mutated glioblastoma with 11C-acetate PET imaging. Journal of Neuro-Oncology, 2019, 145, 441-447.	2.9	8
67	Four "fine―messages from four kinds of "fine―forgotten ligaments of the anterior abdominal wall: have you heard their voices?. Japanese Journal of Radiology, 2019, 37, 750-772.	2.4	8
68	Early and late effects of electroconvulsive therapy associated with different temporal lobe structures. Translational Psychiatry, 2020, 10, 344.	4.8	8
69	Influence of Asthma Onset on Airway Dimensions on Ultra–high-resolution Computed Tomography in Chronic Obstructive Pulmonary Disease. Journal of Thoracic Imaging, 2021, 36, 224-230.	1.5	8
70	Magnetic Resonance Imaging of Sclerosing Lipogranuloma of Male Genitalia. Journal of Urology, 2002, 168, 1500-1501.	0.4	7
71	11C-methylaminoisobutyric acid (MeAIB) PET for evaluation of prostate cancer: compared with 18F-fluorodeoxyglucose PET. Annals of Nuclear Medicine, 2016, 30, 553-562.	2.2	7
72	Uterine peristalsis and junctional zone: correlation with age and postmenopausal status. Acta Radiologica, 2017, 58, 224-231.	1.1	7

#	Article	IF	CITATIONS
73	The role of breast tomosynthesis in a predominantly dense breast population at a tertiary breast centre: breast density assessment and diagnostic performance in comparison with MRI. European Radiology, 2018, 28, 3194-3203.	4.5	7
74	Real-time surveillance of left atrial appendage thrombus during contrast computed tomography imaging for catheter ablation: THe Reliability of cOMputed tomography Beyond UltraSound in THROMBUS detection (THROMBUS) study. Journal of Thrombosis and Thrombolysis, 2019, 47, 42-50.	2.1	7
75	Lobar distribution of non-emphysematous gas trapping and lung hyperinflation in chronic obstructive pulmonary disease. Respiratory Investigation, 2020, 58, 246-254.	1.8	7
76	FDG uptake observed around the lumbar spinous process: relevance to Baastrup disease. Annals of Nuclear Medicine, 2015, 29, 766-771.	2.2	6
77	MR appearance of normal uterine endometrium considering menstrual cycle: differentiation with benign and malignant endometrial lesions. Acta Radiologica, 2016, 57, 1540-1548.	1.1	6
78	What is the most suitable MR signal index for quantitative evaluation of placental function using Half-Fourier acquisition single-shot turbo spin-echo compared with T2-relaxation time?. Acta Radiologica, 2018, 59, 748-754.	1.1	5
79	Synthesis and characterization of a novel <sup>18</sup> F-labeled 2,5-diarylnicotinamide derivative targeting orexin 2 receptor. MedChemComm, 2019, 10, 2126-2130.	3.4	5
80	Dynamics of gyrification in the human cerebral cortex during development. Congenital Anomalies (discontinued), 2017, 57, 8-14.	0.6	4
81	Performance Evaluation of a Newly Developed MR-Compatible Mobile PET Scanner with Two Detector Layouts. Molecular Imaging and Biology, 2020, 22, 407-415.	2.6	4
82	A case of pseudomyxoma peritonei: visualization of septa using diffusion-weighted images with low b values. Abdominal Radiology, 2016, 41, 1713-1717.	2.1	3
83	Intra- and inter-observer agreement in the visual interpretation of interim 18F-FDG PET/CT in malignant lymphoma: influence of clinical information. Acta Radiologica, 2018, 59, 1218-1224.	1.1	3
84	The influence of elevated hormone levels on physiologic accumulation of 68Ga-DOTATOC. Annals of Nuclear Medicine, 2018, 32, 191-196.	2.2	3
85	Characterization of Novel <sup>18</sup> F-Labeled Phenoxymethylpyridine Derivatives as Amylin Imaging Probes. Molecular Pharmaceutics, 2018, 15, 5574-5584.	4.6	3
86	Development of Novel PET Imaging Probes for Detection of Amylin Aggregates in the Pancreas. Molecular Pharmaceutics, 2020, 17, 1293-1299.	4.6	3
87	Qualitative and Quantitative Assessment of Nonlocal Means Reconstruction Algorithm in a Flexible PET Scanner. American Journal of Roentgenology, 2021, 216, 486-493.	2.2	3
88	Signal Intensity and Volume of Pituitary and Thyroid Glands in Preterm and Term Infants. Journal of Magnetic Resonance Imaging, 2021, 53, 1151-1161.	3.4	3
89	Optimization of prediction methods for risk assessment of pathogenic germline variants in the Japanese population. Cancer Science, 2021, 112, 3338-3348.	3.9	3
90	Z-Spectrum Analysis Provides Proton Environment Data (ZAPPED): A New Two-Pool Technique for Human Gray and White Matter. PLoS ONE, 2015, 10, e0119915.	2.5	2

#	Article	IF	CITATIONS
91	Visualization of Magnetization Transfer Effect in Polyethylene Glycol Impregnated Waterlogged Wood. Applied Magnetic Resonance, 2017, 48, 125-134.	1.2	2
92	Enhanced intestinal 2-deoxy-2-[ <sup>18</sup> F]fluoro-D-glucose uptake under metformin is not fully suppressed by loperamide. Endocrine Regulations, 2018, 52, 185-191.	1.3	2
93	Acceleration of 2D-MR fingerprinting by reducing the number of echoes with increased in-plane resolution: a volunteer study. Magnetic Resonance Materials in Physics, Biology, and Medicine, 2020, 33, 783-791.	2.0	2
94	Whole-heart magnetic resonance coronary angiography with multiple breath-holds and automatic breathing-level tracking. Journal of Applied Physics, 2010, 107, 09B308.	2.5	1
95	MR Imaging in Corpus Neoplasia: Spectrum of MR Findings. Current Obstetrics and Gynecology Reports, 2013, 2, 32-42.	0.8	1
96	Adaptive Voxel Matching for Temporal CT Subtraction. Journal of Digital Imaging, 2020, 33, 1543-1553.	2.9	1
97	Imaging reagents study for nuclear medicine using an electron-tracking Compton gamma-ray camera. , 2009, , .		0
98	Imaging study of a phantom and small animal with a two-head electron-tracking Compton gamma-ray camera. , 2010, , .		0
99	Imaging Ovarian Tumor. Nihon Gekakei Rengo Gakkaishi (Journal of Japanese College of Surgeons), 2004, 29, 670-678.	0.0	Ο